Nanoparticle-Mediated Measurement of Target–Drug Binding in Cancer Cells

Adeeti V. Ullal,[†,‡] Thomas Reiner,[†] Katherine S. Yang,[†] Rostic Gorbatov,[†] Changwook Min,[†] David Issadore,[†] Hakho Lee,[†] and Ralph Weissleder[†,§,*]

[†]Center for Systems Biology, Massachusetts General Hospital, 185 Cambridge Street, CPZN 5206, Boston, Massachusetts 02114, United States, [‡]Harvard-MIT Division of Health Sciences and Technology, Massachusetts Institute of Technology, 77 Massachusetts Avenue, E25-519, Cambridge, Massachusetts 02139, United States, and [§]Department of Systems Biology, Harvard Medical School, 200 Longwood Avenue, Boston, Massachusetts 02115, United States

ABSTRACT Responses to molecularly targeted therapies can be highly variable and depend on mutations, fluctuations in target protein levels in individual cells, and drug delivery. The ability to rapidly quantitate drug response in cells harvested from patients in a point-of-care setting would have far reaching implications. Capitalizing on recent developments with miniaturized NMR technologies, we have developed a magnetic nanoparticle-based approach to directly measure both target expression and drug binding in scant human cells. The method involves covalent conjugation of the small-molecule drug to a magnetic nanoparticle that is then used as a read-out for target expression and drug-binding affinity. Using poly(ADP-ribose) polymerase (PARP) inhibition as a model system, we developed an approach to distinguish differential expression of PARP in scant cells with excellent correlation to gold standards, the ability to mimic drug pharmacodynamics *ex vivo* through competitive target–drug binding, and the potential to perform such measurements in clinical samples.

KEYWORDS: nanoparticles · targeting · NMR · DMR · cancer · drugs · PARP

Nanomaterials have become an indispensable tool in the development of clinical diagnostics,[1–3] single-cell analysis,[4,5] and systems-wide analysis of clinical specimens.[6] They can be easily modified with multivalent targeting ligands to amplify signals,[7] improve avidity,[4,5] enhance binding,[8] and translate molecular interactions into measurable electrical, optical, or magnetic signals. In particular, magnetofluorescent nanoparticles allow for dual read-outs by optical (*e.g.*, flow cytometry, immunofluorescence) and magnetic sensing (*e.g.*, nuclear magnetic resonance or magnetoresistive detection). Dextran-coated, cross-linked iron oxide (CLIO) nanoparticles have been shown to be ideal for use with clinical samples, as they are highly stable in physiological buffers and can be easily detected by NMR measurements with low biological background. Recently, our group leveraged these properties to profile scant cells from fine needle aspirate[3] and to enhance detection of rare circulating cancer cells. Most nanoparticle-based diagnostic applications have primarily used antibodies as affinity ligands to detect whole cells,[3] pathogens,[9,10] soluble protein biomarkers,[11] or metabolites.[12]

One major unexplored application has been the use of nanomaterials to quantitatively assay drug–target binding in clinical samples. Although clinical samples are readily procured during routine medical procedures, samples often have scant cells with short half-lives once harvested,[13] thus necessitating a point-of-care assay with minimal sample processing. Tools to quantify target binding in a given patient at a given dose could help in screening drug candidates during pharmaceutical development[14] and also impact treatment decisions made in the clinic. Ultimately such assays would significantly aid in determining whether systemically administered drugs have reached and occupied their intended cellular targets and how target binding varies across patients who may have acquired drug resistance.

In order to enable fast, point-of-care assessment of drug–target interactions, we designed nanosensors that could be adapted to study many drug–targets systems and quickly assayed by a portable diagnostic NMR system (DMR).[9,15] Specifically, we hypothesized that by constructing a single small-molecule drug–nanoparticle conjugate that could compete with corresponding free small molecules for their targets, one could gain insights into the molecular binding action of the drugs. Given the vast repositories of small-molecule drugs, nanosensors could thus be developed for a variety of targets. Furthermore, we reasoned that the drugs themselves could serve as "affinity ligands" and aimed

* Address correspondence to rweissleder@mgh.harvard.edu.

Received for review September 7, 2011 and accepted October 1, 2011.

Published online October 01, 2011
10.1021/nn203450p

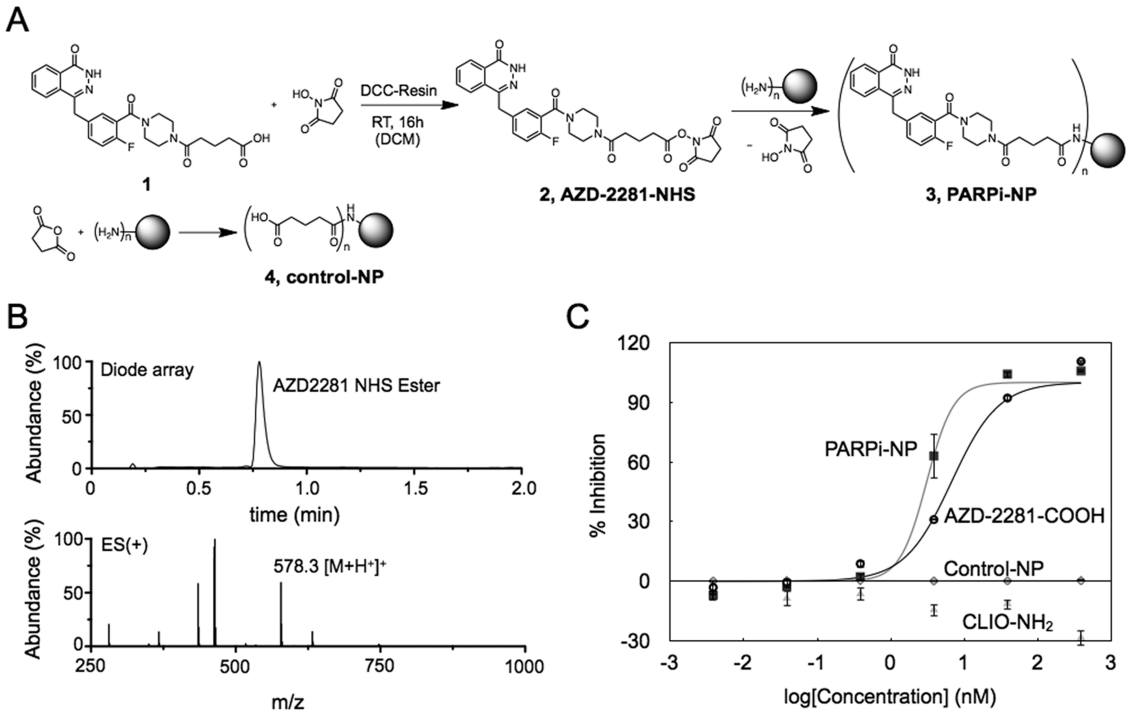

Figure 1. Synthesis and characterization of small-molecule nanoparticles. (a) AZD-2281 was modified to have an NHS-ester and reacted with magnetic nanoparticles (CLIO-NH_2) for 4 h in PBS. A control nanoparticle was created by reacting succinic anhydride with CLIO-NH_2 overnight. (b) HPLC and ESI-LC/MS traces of the AZD-2281 NHS ester. (c) AZD-2281 remained active even after conjugation to CLIO, as verified by a PARP activity assay. $IC_{50,AZD\text{-}COOH}$ = 6.685 nM (5.087 to 8.786 nM IC_{50}, 95% confidence interval; r^2 = 0.9816); $IC_{50,PARPi\text{-}NP}$ = 3.071 nM (1.643 to 5.740 nM IC_{50}, 95% confidence interval; r^2 = 0.9723). Control and unconjugated nanoparticles did not have any inhibitory effect.

at establishing a new biomarker detection paradigm distinct from antibodies.[4] Unlike antibodies, which show binding specificity for single antigenic sites within a given protein, small-molecule drugs bind to specific conformations (*e.g.*, catalytic sites) and often show broader specificity. Using the drug itself as a probe allows for a combined read-out of multiple relevant targets, all of which may affect drug efficacy.

As a model system, we selected poly(ADP-ribose) polymerase (PARP) inhibition and conjugated the PARP inhibitor Olaparib (AZD-2281) to magnetic nanoparticles. Several PARP inhibitors have made significant headway in preclinical and clinical trials for ovarian and breast cancer.[16−19] Moreover, the binding kinetics of PARP inhibitors are particularly interesting, as they have been designed to mimic nicotinamide and competitively block binding at specifically the PARP-1 and PARP-2 catalytic sites.[20] Using the PARP nanosensor, we performed validation experiments, comparative drug inhibition studies, and testing in whole blood samples without the need for prior purification. We show that the method is fast, sensitive, and well suited for point-of-care operation. The ability to measure target binding of an increasing number of molecularly targeted drugs should have a range of applications in biomedicine, drug development, clinical trials, and routine patient care.

RESULTS AND DISCUSSION

Synthesis and Characterization of the PARP Nanosensor. On the basis of earlier findings that the 4-NH-piperazine functionality of AZD-2281 tolerates bulky substituents without significant decrease in binding affinity,[21−23] we chose this site to immobilize the small molecule. For this reason, carboxyl-functionalized precursor **1** was reacted with *N*-hydroxysuccinimide in the presence of a carbodiimide resin, yielding the amine-reactive NHS ester activated AZD-2281 derivative AZD-2281-NHS **2** (Figure 1a). HPLC, ESI-MS, and HRMS spectra confirmed both the identity and purity of the isolated product. AZD-2281-NHS was converted to PARPi-NP **3** by addition of amine-terminated CLIO nanoparticles (Figure 1a). Each nanoparticle had approximately 70 drug molecules covalently attached, which corresponds to near complete conversion of free amine groups on each particle. The AZD-2281 conjugated nanoparticles (PARPi-NPs) were highly stable in solution (>6 months) without detectable aggregation, as determined by dynamic light scattering (mean diameter: 40.1 nm). Control NPs used for all studies were succinylated, but otherwise identical. Carboxylic acid-modified AZD-2281 had an IC_{50} of 6.7 nM, similar to that of the reported free AZD-2281 drug (5 nM).[21,24] Following conjugation to the nanoparticle, the construct retained inhibitory activity against PARP-1 with a measured IC_{50} of 3 nM (Figure 1c). Importantly,

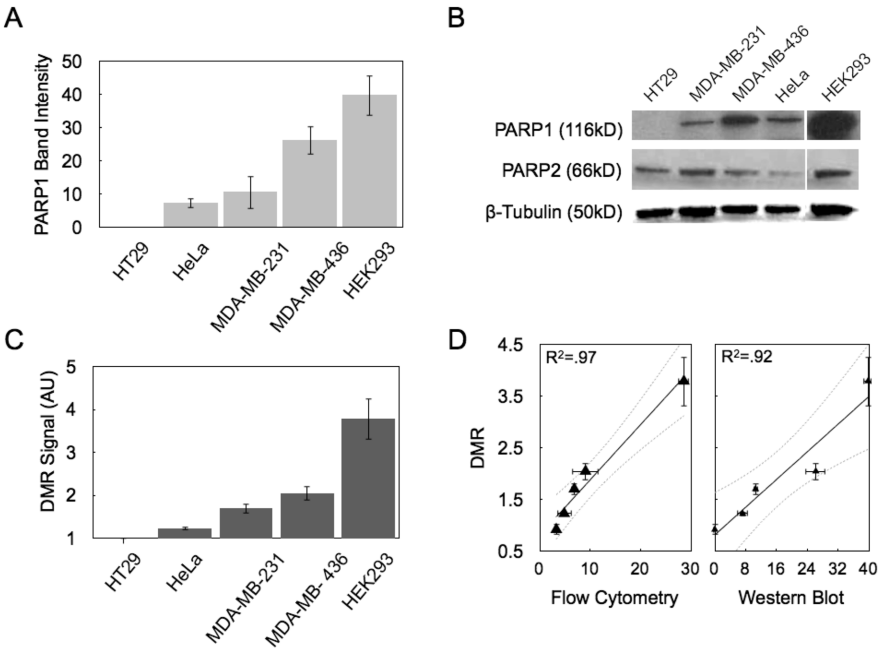

Figure 2. AZD-2281-NP measurement of PARP expression. (a) Cell lines were screened for PARP-1 expression by immunoblotting, and five were selected with varying levels of PARP expression. Expression was quantified from three separate blots and plotted normalized to HT29 expression. (b) Representative Western blot showing PARP-1 and PARP-2 expression. (c) PARPi-NP was applied to the same cell lines to quantify binding to total PARP. Changes in T_2 relaxation time were measured by DMR to measure the amount of magnetic nanoparticle present. The signal of the nanoparticle ($S_{PARPi\text{-}NP}$) was determined by the change compared to PBS ($R_{2,\ NP} - R_{2,\ PBS}$), and this value was normalized to the control NP ($S_{PARPi\text{-}NP}/S_{control\text{-}NP}$). Data shown are in biological duplicate from three separate DMR measurements. (d) PARPi-NP was also optically assayed using flow cytometry (Supporting Information Figure S1) and shows high correlation to DMR measurements (r^2 = 0.97). DMR measurements also had high correlation (r^2 = 0.92) to PARP-1 expression from immunoblotting. Dotted lines represent 95% confidence intervals.

none of the control nanoparticles (either the succinylated or amine precursor CLIO) showed any inhibition of PARP activity. Further characterization of the nanoparticles is included in the Supporting Information (Figure S1).

Validation of the Drug Nanosensor in Cell Lines. We first determined whether the nanosensor could be used to measure PARP expression as well as pharmacological inhibition of PARP by small molecules. We selected five cell lines (HT29, HeLa, MDA-MB-231, MDA-MB-436, and HEK293 cells), which have varying PARP-1 expression levels as confirmed by Western blotting (Figure 2a,b). Cells were fixed, permeabilized, and then incubated with either PARPi-NP or control-NP. The PARPi-NPs had an average diameter of about 40 nm, which is slightly larger than an unconstricted, open nuclear pore size of 30 nm.[25] However, once permeabilized, nanoparticles are able to freely enter the cell by diffusion for both nuclear and cytoplasmic targets.[26] Incubation times and nanoparticle concentrations were selected to achieve maximal target binding from the PARPi-NP with minimal background from the control NP. PARPi-NPs showed tight binding to the target with little decrease in signal over time. Following the removal of excess NPs, samples were processed by the DMR system to determine their transverse relaxation time (T_2). The measured T_2 values were converted to R_2 (=1/T_2) and normalized to PBS and control-NP samples to obtain the PARP-1 cellular expression level (Figure 2c). Figure 2d shows excellent correlation between DMR magnetic measurements and PARP-1 expression levels as determined by Western blots (r^2 = 0.92) and flow cytometry (r^2 = 0.97). DMR measurements were performed with 10 000 cells for validation studies; however, in subsequent experiments signals were detected in as few as 1500 cells. In addition to PARP-1 measurements, we also determined PARP-2 expression levels by immunoblotting (Figure 2b). However, correlation of PARPi-NP to expression was dominated by PARP-1, likely due to the much higher abundance of PARP-1 as compared to PARP-2 in the selected cell lines.

We next used microscopy to further assess quantitative measurements by examining the intracellular localization of nanosensor and drug targets. In HEK293 cells with high PARP expression (Figure 3a), there was excellent co-localization between intracellular PARP-1 antibody and PARPi-NP (co-localization correlation = 0.8). The nanosensor showed strong nucleolar and nuclear localization, which is consistent with PARP-1 subcellular organization, as previously found using PARP-1-expressing cell lines[27,28] or AZD-2281 as a fluorescent probe.[23] Similar trends were observed in HeLa cells, which have moderate PARP-1 expression. In HT29 cells, which have little PARP expression, both the PARP-1 antibody and PARPi-NP showed negligible

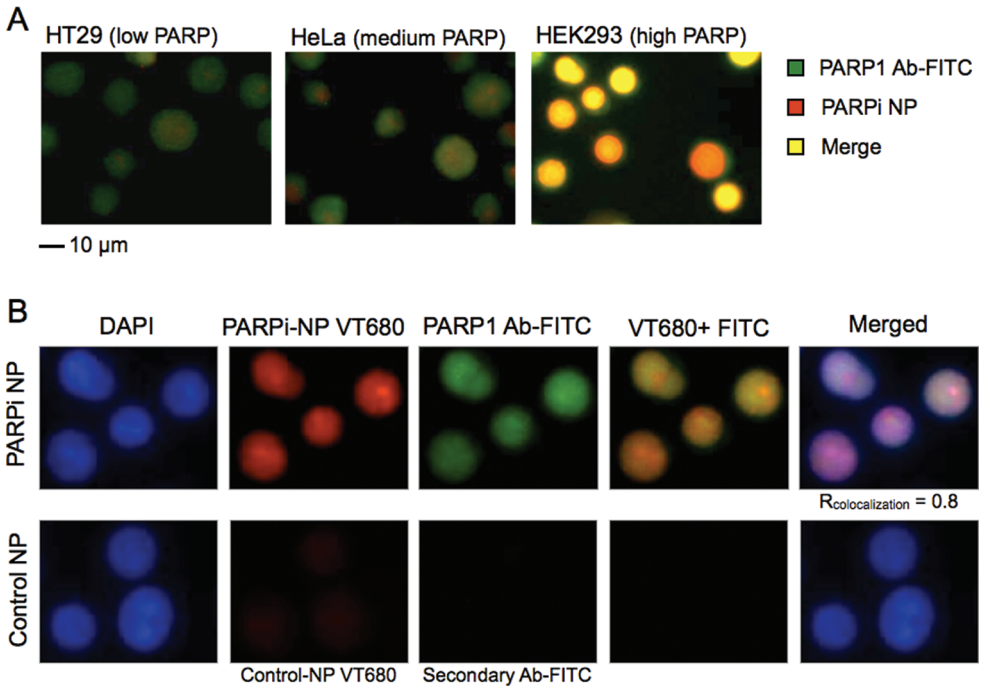

Figure 3. Immunofluorescence of PARPi-NP. (a) Differences in PARP expression could be seen using PARPi-NP and immunofluorescence. Experiments were performed in biological duplicate. PARP-1-Ab is shown in green; PARPi-NP is shown in red, and the merge is displayed in yellow. Here, representative images show that the low PARP expression cell line, HT29, had hardly any PARPi-NP and low PARP-1-Ab binding (mostly background). HeLa cells had slightly more PARP and respectively PARPi-NP. Finally, high PARP expressing HEK283 cells showed high amounts of PARPi-NP and PARP-1-Ab. (b) Strong co-localization of PARPi-NP and PARP-1-Ab was seen (co-localization correlation = 0.8). The control NP had low background with negligible signal.

signal. The control NP showed little to no background (Figure 3b).

Testing Different Small-Molecule PARP Inhibitors Using the Nanosensor. Most small-molecule PARP inhibitors work by competitively inhibiting nicotinamide (NAD+) at the PARP catalytic site.[29] We chose five different, commercially available PARP inhibitors (Figure 4) to test whether the nanosensor-DMR measurements could be used to determine the IC_{50} of each of the different drugs. Briefly, cells were incubated with varying doses of a PARP inhibitor. Subsequently, PARPi-NPs were added to detect the number of unoccupied PARP targets. The entire assay was performed in less than 90 min and required only 10 000 cells. The key PARP inhibitor, AZD-2281, showed an IC_{50} of 1.14 nM and was able to effectively compete with the PARPi-NP in a homologous binding competition assay (Figure 4). AG-014699, which has high structural similarity to AZD-2281, also displayed very tight binding, with an IC_{50} of 0.67 nM. The heterologous competitive binding curve with ABT-888 (Velaparib), another competitive PARP inhibitor, showed an IC_{50} of 9.5 nM. These data suggest that ABT-888 may have a faster off rate than that of PARPi-NP, in turn allowing the PARPi-NP to occupy more PARP sites for a given concentration of free ABT-888. Furthermore, unlike AZD-2281, ABT-888 has been reported to have a slightly stronger binding affinity for PARP-2 as opposed to PARP-1 due to a stronger interaction with α helix-5 in the PARP-2/ABT-888 cocrystal structure.[30] This difference in binding affinity for the two PARP targets could also explain why it has less of a competitive effect on the PARPi-NP compared to AZD-2281 or AG-014699. The weak PARP inhibitor, 3-aminobenzamide, which is similar in structure to NAD+, showed a competitive effect only at extremely high doses (IC_{50} = 29.5 μM). As a negative control, we also demonstrated that the noncompetitive inhibitor BSI-201 (4-iodo-3-nitrobenzamide), which has a distinct pharmacophore and acts by ejecting the first zinc finger of the PARP-1 protein,[31] does not block PARPi-NP binding even at high doses. These results indicate that the nanosensor can indeed be used to quantitate target inhibition in competitive experiments.

Drug Inhibition in Live Cells and Blood Samples. A number of strategies are currently used to measure target binding, including fluorogenic assays, ELISA, radioimmunoassays, mass spectrometry, SILAC, surface plasmon resonance, and isothermal calorimetric measurements. These methods typically require purified target protein, which necessitates a large number of cells and makes it difficult to perform assays under biologically relevant conditions. Consequently, few of these methods are ever performed in a clinical setting where there are time constraints, complexities in obtaining clinical samples, and limited numbers of cells.

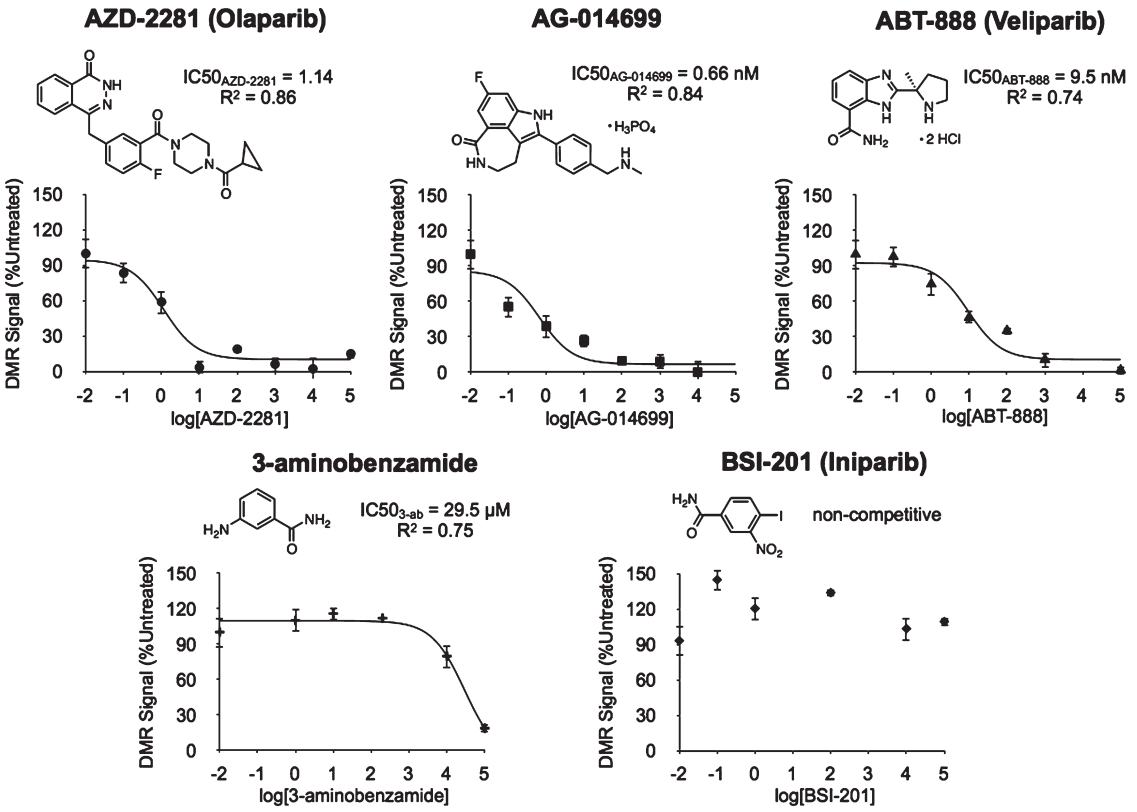

Figure 4. Competitive binding curves of PARPi-NP with various PARP inhibitors. Competitive binding assays were performed by incubating PARP inhibitors designed to compete with nicotinamide at the PARP-1 and PARP-2 catalytic pockets (AZD-2281, AG04699, and ABT888). Another weak competitor, 3-aminobenzamide, was selected, as well as the noncompetitive inhibitor BSI-201 as a negative control. Free PARPi was added at various doses for 30 min before addition of the PARPi-NP or control NP (15 μg Fe/mL). After 20 min of incubation and washing, the signal was read magnetically using DMR. Competitive binding curves were fit using Prism (GraphPad); AZD-2281 had an IC_{50} of 3.4 nM (r^2 = 0.86), AG014699 had an IC_{50} of 7.0 nM (r^2 = 0.84), and ABT-888 had an IC_{50} of 257 nM (r^2 = 0.88). 3-aminobenzamide was only weakly competitive, and BSI-201 had no competitive effect. Experiments were performed on three separate occasions and represent at least biological duplicates. Fluorescence measurements of the PARPi-NP competition assay are included in the Supporting Information (Figure S3).

The simplicity and the robustness of the nanosensor confer potential for the assay to be an effective platform to directly assess drug-binding efficacy in patient samples. To evaluate its clinical utility, we measured target inhibition of AZD-2281 in mock clinical samples. Specifically, the ovarian cancer cell lines A2780, OVCAR429, and UCI-101 or the breast cancer cell line MDA-MB-231 was spiked into human whole blood. The samples were immediately treated with AZD-2281 drug at three different doses: 0 (probing dose), 150 nM (testing dose), and 1.5 μM (saturating dose). We used this "three-dose assay" rather than a full dose response curve (see Figure 4) to speed up analysis and preserve valuable scant clinical samples. After removing excess AZD-2281, the PARPi-NPs were used to probe PARP sites unoccupied by the free drug (Figure 5a). Finally, cancer cells were isolated using CD45 negative selection to remove host cells. While all prior *in vitro* validation DMR assays were performed with 10 000 cells, signals from whole blood samples were detected with as few as 1500 cells. This detection level is promising for clinical samples such as fine needle aspirate, where one obtains about 1500 per pass.[3] Although host cells (CD45+) showed little to no uptake of the PARPi-NP, CD45 negative selection was necessary to reliably detect changes in signal from the PARPi-NP after drug inhibition.

The result at the probing dose ([AZD-2281] = 0 nM; Figure S3a) revealed differences in PARP expression across the cell lines, which could serve as a predictive biomarker for initiating treatment. Indeed, prior work has correlated PARP levels to treatment sensitivity and patient outcome.[32,33] The drug binding levels at the testing and saturating doses were then estimated by comparing R_2 values between drug-treated and untreated samples (Supplementary Figure S4b). At the saturating dose, the binding levels reached a near maximum of 70% in almost all cell lines, except A2780, which showed only moderate drug binding (~40%). At the test dose, however, drug-binding levels varied significantly across tumor lines, presumably reflecting differences in drug uptake as a result of varying expression in drug transporters or variability in binding affinity due to mutations at the catalytic site. We then converted these values into a potential measure of drug-binding efficacy by taking the ratio of drug-binding levels

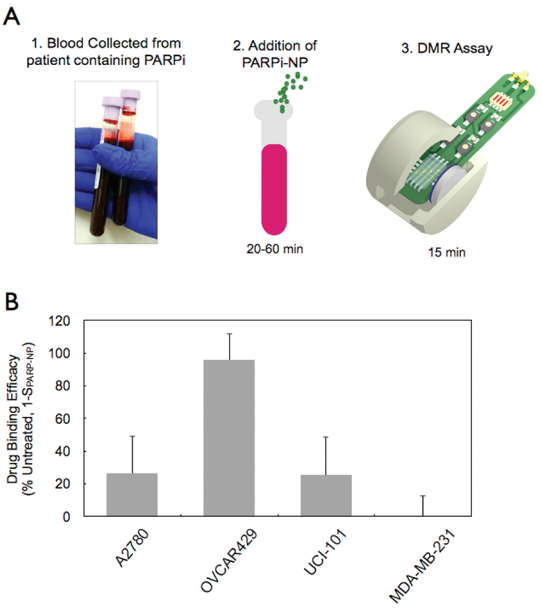

Figure 5. Drug binding efficacy in whole blood samples. (a) Schematic of a clinical drug binding assay from whole blood samples. Mock clinical samples were prepared by spiking cancer cells into human whole blood. This sample was directly incubated with AZD-2281 before the PARPi-NP was added. Quick read-out could then be performed with DMR and/or flow cytometry. (b) Drug-binding levels were determined by looking at the inverse percent change in PARPi-NP from treated *versus* untreated samples. Data shown are an example of "binding efficacy" by taking the ratio of drug bound at the test dose to the saturating dose. OVCAR429 showed the highest drug binding at the test dose and, thus, had a binding efficacy measure of 0.94. In contrast, no drug was bound to MDA-MB-231 at the test dose, resulting in a binding efficacy of 0.00. With further validation, such a measure could be used as a simple diagnostic to dictate treatment choices in the clinic such as choice or dose of drug. Additional measurements of PARP expression and drug-binding levels are included in the Supporting Information (Figure S3).

between the test and the saturating doses (Figure 5b). These results suggest the potential for a future "treatment index", where patients with high drug-binding efficacy would receive lower therapeutic doses, while patients with low drug-binding efficacy would require higher doses or be candidates to receive alternative drugs. In the future we plan to combine this assay with a previously developed assay[26] using two-step antibody–nanoparticle labeling to detect target expression. In this way, we will be able to discriminate low signals as a result of diminished drug binding as opposed to decreased expression of the target protein.

The described approach lays the groundwork for further advances. The sensitivity of the assay could be further enhanced by adopting two-step bioorthogonal systems. In the first step, the drug could compete with a drug–*trans*-cyclooctene (TCO) conjugate of similar size with reduced steric constraints. In a second step, a tetrazine (Tz)-NP could "click" with the drug–TCO to reveal target binding. Such two-step systems have been shown to have a dramatic improvement in sensitivity over direct conjugates;[7] moreover, PARPi-TCO molecules have already been described.[23] A second consideration is the fact that current read-out happens as an average in several hundred to thousands of cells. In the future, we hope to combine the assay with newer generations of ultra-high-sensitivity DMR and other magnetic technologies that would allow for single-cell sensing of drug binding.[15] This sensitivity could potentially allow for early identification of rare drug-resistant clones where the target protein contains mutations in the drug-binding pocket or the resistant cells display an increase in drug efflux pumps. Finally, in the current work we have focused solely on drug target binding, but not on therapeutic efficacy. It would thus be of interest to combine the current assay with molecular profiling of several protein biomarkers to measure drug response. For example, one could assay cellular phenotypes to drug response such as apoptosis induction *via* measurements of cleaved caspases and cleaved PARP or PI3K/MAP kinase inhibition using measurements of key signaling pathway proteins such as phospho-s6rp.[26]

We believe that the described method could serve as a broader platform generalizeable to other drugs and their targets. The main challenges in adapting the assay to other drug or cellular systems are (1) the ability to modify the drug while retaining target specificity, tight binding, and stability in aqueous buffers and (2) optimization of assay conditions to ensure optimal nanoparticle binding for each target system. For target proteins with small binding pockets, steric hindrance from the nanoparticles may be an issue. This could be overcome by implementing two-step labeling with click chemistries. Recently, we have shown this to be possible for a variety of targets, *e.g.*, Taxol,[34] PARP-1,[22,35,36] or PLK1 inhibitors.[37] Each target–inhibitor system would also require optimization of drug and nanoparticle concentrations, incubation times, and cell permeabilization levels to ensure that nanoparticle binding is not assay-limited. Notably, an inherent benefit of the assay is that just one drug conjugate is required to survey several inhibitors of a particular target (Figure 4). Thus, there is flexibility during assay development to select a drug that is both optimal for the target system and easy to work with. In the future, we believe the assay can be extended beyond cancer cells and used in other disease states and even other organisms such as bacteria to assay antibiotic resistance.

The ability to provide such data in biologically relevant samples could be of considerable clinical interest to make rational treatment decisions, optimize doses in a given patient, and understand population heterogeneities of drug responses. The method could also serve to quantitate the effective drug target resident time in readily accessible samples such as peripheral blood. In sum, we designed

and developed a paradigm using small-molecule nanoparticle conjugates that have the potential to address several clinical limitations and to impact patient treatment.

MATERIALS AND METHODS

Materials. The cell lines HT29, MDA-MB-231, MDA-MB-436, HeLa, HEK293, UCI-101, A2780, and OVCAR429 were all obtained from ATCC and cultured in RPMI (MDA-MBA-231, MDA-MB-436, OVCAR429, A2780, UCI-101) or DMEM (HT29, HeLa, HEK293) with 10% fetal bovine serum, 1% L-glutamine, and 1% penicillin. Free AZD-2281 (Selleck), BSI-201 (ChemieTek), AG-014699 (ChemieTek), ABT-888 (ChemieTek), and 3-aminobenzamide (Sigma) were all commercially purchased for use in competition assays. Until otherwise noted, all reagents were purchased from Sigma-Aldrich (St. Louis, MO) and used without further purification. Cyclohexylcarbodiimide polystyrene resin was purchased from EMD Biosciences (Gibbstown, NJ, USA). 4-[[4-Fluoro-3-(4-(5-oxopentanamide)piperazine-1-carbonyl) phenyl]methyl]-2*H*-phthalazin-1-one was synthesized according to published literature procedures.[23] Proton nuclear magnetic resonance (^{1}H NMR) spectra were recorded on a Varian AS-400 (400 MHz) spectrometer. Chemical shifts for protons are reported in parts per million (ppm) and are referenced against the dimethylsulfoxide lock signal (^{1}H, 2.50 ppm). Data are reported as follows: chemical shift, multiplicity (s = singlet, d = doublet, t = triplet, m = multiplet), coupling constants, and integration. LC-ESI-MS analysis and HPLC purifications were performed on a Waters (Milford, MA, USA) LC-MS system. For LC-ESI-MS analyses, a Waters XTerra C18 5 μm column was used. For preparative runs, an Atlantis Prep T3 OBD 5 μM or a XTerra Prep MS C18 OBD 5 μM column was used. High-resolution electrospray ionization (ESI) mass spectra were obtained on a Bruker Daltonics APEXIV 4.7 T Fourier transform mass spectrometer (FT-ICR-MS) in the Department of Chemistry Instrumentation Facility at the Massachusetts Institute of Technology.

Synthesis of AZD-2281-NHS. Cyclohexylcarbodiimide polystyrene resin (74 mg, 2.3 mmol/g) was added to a solution of 4-[[4-fluoro-3-(4-(5-oxopentanamide)piperazine-1-carbonyl)phenyl] methyl]-2*H*-phthalazin-1-one (**1**) (20 mg, 0.042 mmol) and *N*-hydroxysuccinimide (20 mg, 0.174 mmol) in dichloromethane (1.5 mL), and the resulting mixture stirred gently at room temperature overnight. Subsequently, the reaction mixture was filtered and volatiles were removed *in vacuo*. The crude material was purified via silica chromatography (acetonitrile/ethyl acetate = 5−100%), yielding the title compound as a clear solid (15.5 mg, 0.027 mmol, 64%): ^{1}H NMR (400 MHz, DMSO-d_6) δ 12.59 (s, 1H), 8.26 (d, $^3J_{HH}$ = 7.7, 1H), 7.96 (d, $^3J_{HH}$ = 7.9, 1H), 7.89 (t, $^3J_{HH}$ = 7.2, 1H), 7.83 (t, $^3J_{HH}$ = 7.4, 1H), 7.47−7.41 (m, 1H), 7.39−7.34 (m, 1H), 7.24 (t, $^3J_{HH}$ = 9.0, 1H), 4.33 (s, 2H), 3.67−3.12 (m, 8H), 2.81 (m, 4H), 2.72 (t, $^3J_{HH}$ = 6.4, 2H), 2.50−2.40 (m, 2H), 1.89−1.81 (m, 2H); ^{19}F NMR (376 MHz, DMSO-d_6) δ −119.68; LC-ESI-MS(−) m/z = 576.2 $[M - H]^-$; LC-ESI-MS(+) m/z = 578.3 $[M + H]^+$; HRMS-ESI $[M - H]^+$ m/z calcd for $[C_{29}H_{27}FN_5O_7]^-$ 576.1900, found 576.1888.

NP Synthesis. Cross-linked iron oxide nanoparticles were synthesized and tagged with an amine reactive cyanine dye (VivoTag 580xL, VT680xL, Perkin-Elmer) as previously described.[7] Magnetofluorescent nanoparticles were reacted with 370 equivalents of AZD-2281-NHS (**2**) in PBS with 5% dimethylformamide for 4 h at room temperature. Excess AZD-2281-NHS was removed using 100 kD ultracentrifugation filtration units (Amicon), washed three times with PBS at 2000 rcf for 10 min, and subsequently passed through a Sephadex G50 column.

NP Characterization. Nanoparticle concentration was determined by measuring iron content through absorbance at a characteristic wavelength of 400 nm as previously established.[38,39] Drug loading was determined by measuring the change in absorbance between the conjugated and unconjugated nanoparticle at 275 nm. This change in absorbance was normalized by the amount of CLIO per sample, as calculated previously using iron concentration (UV absorbance at 400 nm).[38] Molecules of AZD-2281 per nanoparticle were determined using a standard curve for the unreacted AZD-2281-NHS-ester. Drug inhibitory activity was confirmed by testing the ability of AZD-2281-NP to inhibit PARP activity using a standard, *in vitro* plate assay (Trevigen). Nanoparticle size was measured using dynamic light scattering (Malvern) (Figure S1).

Cell Labeling. Cells were grown in culture for 3 days up to 90% confluency before collection with 0.05% Trypsin/0.53 mM EDTA and washed once with stain buffer, SB+ (PBS + 2% FBS + 1% BSA). Cells were then fixed with a 1:1 mixture of PBS with a formaldehyde-based fix buffer (FBI, BD Biosciences) for 20 min at room temperature and permeabilized by washing twice with a saponin-containing buffer with 1% BSA (PW+) (Perm/Wash Buffer, BD Biosciences). Each sample (250 000 cells/sample) was then labeled with 15 μg Fe/mL of nanoparticle (PARPi-NP or control NP) in PW+ and incubated at room temperature protected from light on a rocker for 20 min. Excess nanoparticle was removed with two washes of PW+ before a final wash and resuspension in PBS (or stain buffer).

For the competition assay, HEK293 cells were treated with varying concentrations from 0 to 100 μM of various PARP inhibitors. Solutions were made up in PW+. After a 20 min incubation at room temperature with the free inhibitor, the targeted PARPi-NP or control NP was added to the same mix for a total concentration of 15 μg Fe/mL and incubated for an additional 20 min before washing and continuing with labeling as described above. Data shown represent at least biological duplicates, and experiments were repeated at least three times. All data were fitted using Prism 5.0 (GraphPad, La Jolla, CA, USA).

Immunoblotting. Lysates were collected from cells at 90% confluency by washing with cold PBS on ice and scraping with Ripa buffer containing a protease inhibitor cocktail. Samples were syringed 3 to 5 times and sonicated for 30 s before being spun down at 10 000 rpm for 15 min to collect the supernatant. Samples were made up with 4× Laemlli buffer with DTT and boiled for 10 min. A 10 μg sample of total protein was loaded on NuPAGE 4−12% gradient Bis-Tris gels (Invitrogen) with MOPS running buffer and transferred to a PVDF membrane using an iBlot gel transfer device (Invitrogen). Blots were blocked with 5% dried milk in TBST (TBS with 0.1% Tween-20) and probed with primary monoclonal antibodies at the appropriate dilutions (PARP-1, Santa Cruz Biotechnology sc7150, 1:250; PARP-2, Abcam ab93416, 1:250; Beta-tubulin, Abcam ab7287, 1:100). Relative expression for each blot was quantified using ImageJ (NIH).To ensure consistency in PARP expression, cell lysates were collected within four passages of the PARPi-NP detection. Data shown are representative of biological triplicates and are displayed as mean ± standard error.

Flow Cytometry. To determine target binding, the amount of nanoparticle present was quantified from VT680 fluorescence with an LSRII flow cytometer (Becton Dickinson), and the geometric mean of fluorescence intensity was determined using FlowJo software. All measurements were performed in biological triplicate, and signals were normalized by the control NP sample ($S_{PARPi\text{-}NP}/S_{Control\text{-}NP}$). Data are shown as mean ± standard error.

Microscopy. Cells were labeled with nanoparticle as described above and then incubated for 1 h at room temperature with a PARP-1 antibody (Santa Cruz Biotechnology sc8007) at a dilution of 1:50 in PW+. Cells were washed once with PW+ and then incubated with secondary antibody at 2 μg/mL for half an hour on ice. Cells were washed two more times with PW+ before resuspension in PBS. A minimal volume (100 μL) of sample containing approximately 10 000 cells was transferred to a 96-well plate and imaged. Images were acquired at 40× with a DeltaVision screening system (Applied Precision Instruments) and analyzed using FIJI software (version 1.45).

DMR. Magnetic detection measurements were conducted as described previously[3] with 10 000 cells using the miniaturized nuclear magnetic resonance device, DMR,[9] for target expression and competitive binding experiments. Detection in whole blood studies was performed with detection of as few as 1500 cells. Signals were calculated by converting T_2 measurements to R_2 and comparing the change in R_2 from the baseline PBS sample to the labeled PARPi-NP ($S_{PARPi\text{-}NP}$) or control-NP ($S_{Control\text{-}NP}$). Signals from the PARPi-NP were normalized by dividing by the signal from the control NP ($S_{PARPi\text{-}NP}/S_{Control\text{-}NP}$). Data shown are in biological duplicate and are represented as means ± standard error.

Whole Blood Processing. Selected cell lines (A2780, UCI-101, OVCAR429, and MDA-MB-231) were spiked into human whole blood samples (200 000 cells in 1.5 mL). Samples were then either left untreated or incubated with AZD-2281 at 155 nM and 1.5 μM for 30 min at room temperature. Following drug incubation, red blood cells were partially lysed with an RBC lysis agent (Qiagen), and the sample was washed with SB+. The sample was then divided into two samples and probed with either PARPi-NP or control NP at 5 μg Fe/mL in 0.2× PW+ for 60 min. Samples were washed twice with 0.2× PW+ before resuspension in SB+ (or PBS). CD45 negative selection was performed by using CD45 magnetic beads and LS columns (Miltenyi Biotec). Signals from CD45+ cell samples were then measured by flow cytometry or DMR.

Acknowledgment. The authors thank N. Sergeyev for synthesizing the CLIO, B. Marinelli and K. Snyder for assisting with DMR measurements, J. Dunham with imaging, M. Etzrodt and V. Cortez-Retamozo for assistance with flow cytometry experiments, and C. Tassa and M. Liong for guidance on nanoparticle conjugations. We especially thank G. Thurber and J. Haun for many helpful discussions. A.V.U. was supported in part by an NSF fellowship. T.R. was supported by a grant from the German National Academy of Sciences Leopoldina (LPDS 2009-24). This work was supported in part by National Institutes of Health Grants R01-EB0044626, R01-EB010011, P50 grant P50CA86355, U54CA151884, and TPEN contract HHSN268201000044C.

Supporting Information Available: Nanoparticle characterization and additional data from flow cytometry experiments are included in supplementary figures. This material is available free of charge via the Internet at http://pubs.acs.org.

REFERENCES AND NOTES

1. Giljohann, D. A.; Mirkin, C. A. Drivers of Biodiagnostic Development. *Nature* **2009**, *462*, 461–464.
2. Cheng, M. M.; Cuda, G.; Bunimovich, Y. L.; Gaspari, M.; Heath, J. R.; Hill, H. D.; Mirkin, C. A.; Nijdam, A. J.; Terracciano, R.; Thundat, T.; *et al*. Nanotechnologies for Biomolecular Detection and Medical Diagnostics. *Curr. Opin. Chem. Biol.* **2006**, *10*, 11–19.
3. Haun, J. B.; Castro, C. M.; Wang, R.; Peterson, V. M.; Marinelli, B. S.; Lee, H.; Weissleder, R. Micro-NMR for Rapid Molecular Analysis of Human Tumor Samples. *Sci. Transl. Med.* **2011**, *3*, 71ra16.
4. Tassa, C.; Duffner, J. L.; Lewis, T. A. Binding Affinity and Kinetic Analysis of Targeted Small Molecule-Modified Nanoparticles. *Bioconjugate Chem.* **2009**, *21*, 14–19.
5. Hong, S.; Leroueil, P.; Majoros, I.; Orr, B.; Baker, J.; Holl, M. The Binding Avidity of a Nanoparticle-Based Multivalent Targeted Drug Delivery Platform. *Chem. Biol.* **2007**, *14*, 107–115.
6. Fan, R.; Vermesh, O.; Srivastava, A.; Yen, B. K.; Qin, L.; Ahmad, H.; Kwong, G. A.; Liu, C. C.; Gould, J.; Hood, L.; *et al*. Integrated Barcode Chips for Rapid, Multiplexed Analysis of Proteins in Microliter Quantities of Blood. *Nat. Biotechnol.* **2008**, *26*, 1373–1378.
7. Haun, J. B.; Devaraj, N. K.; Hilderbrand, S. A.; Lee, H.; Weissleder, R. Bioorthogonal Chemistry Amplifies Nanoparticle Binding and Enhances the Sensitivity of Cell Detection. *Nat. Nanotechnol.* **2010**, *5*, 660–665.
8. Shaw, S. Y.; Westly, E. C.; Pittet, M. J.; Subramanian, A.; Schreiber, S. L.; Weissleder, R. Perturbational Profiling of Nanomaterial Biologic Activity. *Proc. Natl. Acad. Sci. U. S. A.* **2008**, *105*, 7387–7392.
9. Lee, H.; Sun, E.; Ham, D.; Weissleder, R. Chip-Nmr Biosensor for Detection and Molecular Analysis of Cells. *Nat. Med.* **2008**, *14*, 869–874.
10. Lee, H.; Yoon, T. J.; Weissleder, R. Ultrasensitive Detection of Bacteria Using Core-Shell Nanoparticles and an Nmr-Filter System. *Angew. Chem., Int. Ed. Engl.* **2009**, *48*, 5657–5660.
11. Perez, J. M.; Josephson, L.; O'Loughlin, T.; Hogemann, D.; Weissleder, R. Magnetic Relaxation Switches Capable of Sensing Molecular Interactions. *Nat. Biotechnol.* **2002**, *20*, 816–820.
12. Sun, E. Y.; Weissleder, R.; Josephson, L. Continuous Analyte Sensing with Magnetic Nanoswitches. *Small* **2006**, *2*, 1144–1147.
13. Stott, S. L.; Lee, R. J.; Nagrath, S.; Yu, M.; Miyamoto, D. T.; Ulkus, L.; Inserra, E. J.; Ulman, M.; Springer, S.; Nakamura, Z.; *et al*. Isolation and Characterization of Circulating Tumor Cells from Patients with Localized and Metastatic Prostate Cancer. *Sci. Transl. Med.* **2010**, *2*, 25ra23.
14. Swinney, D. C.; Anthony, J. How Were New Medicines Discovered? *Nat. Rev. Drug. Discov.* **2011**, *10*, 507–519.
15. Issadore, D.; Min, C.; Liong, M.; Chung, J.; Weissleder, R.; Lee, H. Miniature Magnetic Resonance System for Point-of-Care Diagnostics. *Lab Chip* **2011**, *11*, 2282–2287.
16. Johnson, N.; Li, Y. C.; Walton, Z. E.; Cheng, K. A.; Li, D.; Rodig, S. J.; Moreau, L. A.; Unitt, C.; Bronson, R. T.; Thomas, H. D.; *et al*. Compromised Cdk1 Activity Sensitizes Brca-Proficient Cancers to PARP Inhibition. *Nat. Med.* **2011**, *17*, 875–882.
17. Dedes, K. J.; Wetterskog, D.; Mendes-Pereira, A. M.; Natrajan, R.; Lambros, M. B.; Geyer, F. C.; Vatcheva, R.; Savage, K.; Mackay, A.; Lord, C. J.; *et al*. Pten Deficiency in Endometrioid Endometrial Adenocarcinomas Predicts Sensitivity to PARP Inhibitors. *Sci. Transl. Med.* **2010**, *2*, 53ra75.
18. O'Shaughnessy, J.; Osborne, C.; Pippen, J. E.; Yoffe, M.; Patt, D.; Rocha, C.; Koo, I. C.; Sherman, B. M.; Bradley, C. Iniparib Plus Chemotherapy in Metastatic Triple-Negative Breast Cancer. *N. Engl. J. Med.* **2011**, *364*, 205–214.
19. Tutt, A.; Robson, M.; Garber, J. E.; Domchek, S. M. Oral Poly (Adp-Ribose) Polymerase Inhibitor Olaparib in Patients with Brca1 or Brca2 Mutations and Advanced Breast Cancer: A Proof-of-Concept Trial. *The Lancet* **2010**.
20. He, J. X.; Yang, C. H.; Miao, Z. H. Poly(Adp-Ribose) Polymerase Inhibitors as Promising Cancer Therapeutics. *Acta Pharmacol. Sin.* **2010**, *31*, 1172–1180.
21. Menear, K. A.; Adcock, C.; Boulter, R. 4-[3-(4-Cyclopropanecarbonylpiperazine-1-Carbonyl)-4-Fluorobenzyl]-2H-Phthalazin-1-One: A Novel Bioavailable Inhibitor of Poly-(Adp-Ribose) Polymerase-1. *J. Med. Chem.* **2008**, *51*, 6581–6591.
22. Keliher, E. J.; Reiner, T.; Turetsky, A.; Hilderbrand, S. A.; Weissleder, R. High-Yielding, Two-Step 18f Labeling Strategy for 18f-Parp1 Inhibitors. *ChemMedChem* **2011**, *6*, 424–427.
23. Reiner, T.; Earley, S.; Turetsky, A.; Weissleder, R. Bioorthogonal Small-Molecule Ligands for Parp1 Imaging in Living Cells. *Chembiochem* **2010**, *11*, 2374–2377.
24. Ferraris, D. V. Evolution of Poly (Adp-Ribose) Polymerase-1 (Parp-1) Inhibitors. From Concept to Clinic. *J. Med. Chem.* **2010**, *53*, 4561–4584.
25. Alber, F.; Dokudovskaya, S.; Veenhoff, L. M.; Zhang, W.; Kipper, J.; Devos, D.; Suprapto, A.; Karni-Schmidt, O.; Williams, R.; Chait, B. T. The Molecular Architecture of the Nuclear Pore Complex. *Nature* **2007**, *450*, 695–701.
26. Haun, J. B.; Devaraj, N. K.; Marinelli, B. S.; Lee, H.; Weissleder, R. Probing Intracellular Biomarkers and Mediators of Cell Activation Using Nanosensors and Bioorthogonal Chemistry. *ACS Nano* **2011**, *5*, 3204–3213.
27. Haince, J. F.; McDonald, D.; Rodrigue, A.; Dery, U.; Masson, J. Y.; Hendzel, M. J.; Poirier, G. G. Parp1-Dependent Kinetics of Recruitment of Mre11 and Nbs1 Proteins to Multiple DNA Damage Sites. *J. Biol. Chem.* **2008**, *283*, 1197–1208.
28. Meder, V. S.; Boeglin, M.; de Murcia, G.; Schreiber, V. Parp-1 and Parp-2 Interact With Nucleophosmin/B23 and Accumulate in Transcriptionally Active Nucleoli. *J. Cell Sci.* **2005**, *118*, 211–222.

29. Miyashiro, J.; Woods, K. W.; Park, C. H.; Liu, X.; Shi, Y.; Johnson, E. F.; Bouska, J. J.; Olson, A. M.; Luo, Y.; Fry, E. H.; *et al*. Synthesis and SAR of Novel Tricyclic Quinoxalinone Inhibitors of Poly(Adp-Ribose)Polymerase-1 (Parp-1). *Bioorg. Med. Chem. Lett.* **2009**, *19*, 4050–4054.
30. Karlberg, T.; Hammarstrom, M.; Schutz, P.; Svensson, L.; Schuler, H. Crystal Structure of the Catalytic Domain of Human Parp2 in Complex with Parp Inhibitor Abt-888. *Biochemistry* **2010**, *49*, 1056–1058.
31. Mendeleyev, J.; Kirsten, E.; Hakam, A.; Buki, K. G.; Kun, E. Potential Chemotherapeutic Activity of 4-Iodo-3-Nitrobenzamide: Metabolic Reduction to the 3-Nitroso Derivative and Induction of Cell Death in Tumor Cells in Culture. *Biochem. Pharmacol.* **1995**, *50*, 705–714.
32. Brustmann, H. Poly(Adenosine Diphosphate-Ribose) Polymerase Expression in Serous Ovarian Carcinoma: Correlation with P53, Mib-1, and Outcome. *Int. J. Gynecol. Pathol.* **2007**, *26* (2), 147–153.
33. von Minckwitz, G.; Müller, B. M.; Loibl, S.; Budczies, J.; Hanusch, C.; Darb-Esfahani, S.; Hilfrich, J.; Weiss, E.; Huober, J.; Blohmer, J. U. Cytoplasmic Poly(Adenosine Diphosphate–Ribose) Polymerase Expression is Predictive and Prognostic in Patients with Breast Cancer Treated with Neoadjuvant Chemotherapy. *J. Clin. Oncol.* **2011**, *29*, 2150.
34. Devaraj, N. K.; Hilderbrand, S.; Upadhyay, R.; Mazitschek, R.; Weissleder, R. Bioorthogonal Turn-On Probes for Imaging Small Molecules Inside Living Cells. *Angew. Chem.* **2010**, *122*, 2931–2934.
35. Reiner, T.; Kohler, R. H.; Liew, C. W.; Hill, J. A.; Gaglia, J.; Kulkarni, R. N.; Weissleder, R. Near-Infrared Fluorescent Probe for Imaging of Pancreatic B Cells. *Bioconjugate Chem.* **2010**, *21*, 1362–1368.
36. Reiner, T.; Keliher, E. J.; Earley, S.; Marinelli, B.; Weissleder, R. Synthesis and in Vivo Imaging of a 18f-Labeled Parp1 Inhibitor Using a Chemically Orthogonal Scavenger-Assisted High-Performance Method. *Angew. Chem., Int. Ed.* **2011**, *50*, 1922–1925.
37. Budin, G.; Yang, K. S.; Reiner, T. Bioorthogonal Probes for Polo-Like Kinase 1 Imaging and Quantification. *Angew. Chem.* **2011**, *50* (40), 9378–9381.
38. Tassa, C.; Shaw, S. Y.; Weissleder, R. Dextran-Coated Iron Oxide Nanoparticles: A Versatile Platform for Targeted Molecular Imaging, Molecular Diagnostics, and Therapy *Acc. Chem. Res.* **2011**, Doi: 10.1021/ar200084x.
39. Reynolds, F.; O'Loughlin, T.; Weissleder, R.; Josephson, L. Method of Determining Nanoparticle Core Weight. *Anal. Chem.* **2005**, *77*, 814–817.